THE CHARACTERISTICS OF TOTAL ELECTRON CONTENT DISTURBANCES AT LOW LATITUDES DURING SEVERE GEOMAGNETIC STORM EVENTS ON MARCH 24 AND APRIL 24, 2023

Chollada Pansong[1]*, Samatchaya Maichuen[2], and Pattawut Wongsak[2]
E-mail: chollada_p@rmutt.ac.th[1*], 67036099@kmitl.ac.th[2], and 67036098@kmitl.ac.th[2]

Received: August 16, 2024
Revised: October 14, 2024
Accepted: November 25, 2024

ABSTRACT

This study investigated the Total Electron Content (TEC) characteristics at two different low latitudes and three different TEC sources during the severe geomagnetic storms, focusing on the events of March 24, 2023, and April 24, 2023. TEC data were collected from GNSS receivers in Chumphon (THCP station: 10.724°N, 99.375°E), and Bangkok (THBK station: 13.729°N, 100.780°E), Thailand, using three sources: GNSS satellite receivers, the International GNSS Service (IGS), and the International Reference Ionosphere (IRI). GPS TEC, IGS TEC, and IRI TEC values were compared among them. The correlation coefficient between geomagnetic storm intensity and ionospheric TEC disturbances was analyzed. The results show that geomagnetic storm levels strongly influence ionospheric TEC disturbances. TEC values typically increase during storms and return to normal within a few days. During the storm events, TEC increased up to 75% over Chumphon and 10-35% over Bangkok. The strong geomagnetic storms exhibited positive correlations with higher TEC values, while quiet periods showed no significant decreases below baseline levels, indicating a negative correlation coefficient.

Keywords: Geomagnetic storm, GPS TEC, IGS TEC, IRI TEC, Low latitude

*Corresponding author E-mail: chollada_p@rmutt.ac.th
[1*]Department of Technical Education, Faculty of Technical Education, Rajamangala University of Technology Thanyaburi, Pathum Thani, 12110 Thailand
[2]Department of Engineering Education, School of Industrial Education and Technology, King Mongkut's Institute of Technology Ladkrabang, Bangkok, 10520 Thailand

I. INTRODUCTION

The Global Navigation Satellite System (GNSS) provides a reliable reference and a novel approach for sensing natural dynamics. One of its components, the Global Positioning System (GPS), relies on signal quality affected by electron diffusion in the ionosphere (Chernyshov et al., 2020, p. 1). The ionosphere, as a propagation medium, slows signal transmission depending on plasma density. Disturbances in the ionosphere negatively impact GPS accuracy and reliability, with free electrons influencing signal phase and amplitude. The ionosphere's Total Electron Content (TEC) affects the group delay and phase advance of GPS signals, with higher TEC values causing a more significant signal impact. Irregular plasma density leads to wave distortion, resulting in inaccurate parameter estimation or temporary signal interruptions (slips). Ionospheric anomalies arise from disturbances in Earth's space environment caused by solar and geophysical factors. Influences such as the Interplanetary Magnetic Field (IMF), solar wind, geomagnetic storms, and sub-storms contribute to near-Earth plasma conditions and their relation to solar activity (Hofmann-Wellenhof et al., 1992, pp. 90-97; Pi et al., 1997, p. 2283; Skone & de Jong, 2000, p. 1067; Chernyshov et al., 2020, p. 1; Tsurutani et al., 2020).

Positive ionospheric storms are linked to enhanced electron density caused by thermospheric winds, compositional changes, ionization, and electric field transport. In contrast, negative storms primarily result from compositional changes in the ionosphere (Nayak et al., 2016, pp. 7941-7960; Reddybattula et al., 2019, p. 283; Serafimov et al., 1982, pp. 397-399). TEC disturbances caused by geomagnetic storms vary with latitude. At low latitudes, electromagnetic fields strongly influence TEC over the magnetic equator, leading to increased electrical conductivity (Li et al., 2019, p. 9380). During storms, ionospheric currents and energetic particles release heat energy, elevating and redistributing atmospheric density, which increases drag on low-Earth orbit satellites. The ionosphere is classified into high-, mid-, low-latitude, and equatorial regions. Low-latitude and equatorial regions (±20° of the geomagnetic equator) exhibit high electron density and complex variations caused by phenomena such as the Equatorial Ionization Anomaly (EIA) and Equatorial Electrojet (EEJ). Research on these regions is vital for understanding ionospheric morphology and improving modeling techniques (Jenan et al., 2021, pp. 575-587; Kumar et al., 2016, pp. 1755-1762; Reddy, 1986, pp. 247-263).

Previous studies include Kenpankho et al. (2011, pp. 365-370), who compared GPS TEC and IRI predictions at Chumphon; Rao et al. (2013, pp. 1-6), who studied TEC variability along 73°E; and Nava et al. (2016, pp. 3421-3438), who analyzed mid- and low-latitude ionospheric responses to the 2015 St. Patrick's Day storm. Zhou et al. (2016, pp. 9146-9163) investigated ionospheric storm effects during the March 2015 event, while Chen et al. (2017, pp. 3632-3639) examined geomagnetic activity's influence on TEC using different analytical methods. Reddybattula et al. (2019, p. 283) analyzed TEC during various geomagnetic storm intensities in India, and de Paula et al. (2019, pp. 1-15) studied ionospheric irregularities over Brazil during the September 2017 storm. Additional research includes Dugassa et al. (2019, pp. 1161-1180), who examined TEC gradients and irregularities; Mansilla (2019, pp. 26-36), who studied TEC behavior in polar regions during intense storms; and Ali et al. (2021, pp. 4857-4871), who analyzed transient TEC variations at low latitudes. Ratovsky et al. (2022, pp. 1-15) linked extreme ionospheric events to geomagnetic activity, while Klimenko et al. (2017, pp. 923-938) reported on similarities and differences in morphology and mechanisms of the foF2 and TEC disturbances during the geomagnetic storms on September 26-30, 2011. Machine learning-based TEC modeling during storms was explored by Adolfs et al. (2022, pp. 1-17).

Finally, Bojilova and Mukhtarov (2023, pp. 1-23) analyzed global and regional ionospheric responses during the February 2022 storms. After reviewing relevant studies, we designed research to investigate, analyze, and compare low-latitude TEC disturbances over Bangkok and Chumphon, Thailand, during the severe geomagnetic storms of March 24, 2023, and April 24, 2023. TEC data were collected from three sources: GPS, the International GNSS Service (IGS), and the International Reference Ionosphere (IRI), to conduct a comprehensive analysis of these disturbances. Chen et al. (2017, pp. 3632-3639) examined the impact of geomagnetic activity on TEC data, comparing the Spectral Whitening Method (SWM) and the 28-day Running Median Centered (RMC) technique. They found that RMC overestimated disturbances by 5–20% during geomagnetic storms and up to 35% during quiet conditions compared to SWM. Similarly, Nava et al. (2016, pp. 3421-3438) analyzed ionospheric responses at mid- and low latitudes during the 2015 St. Patrick's Day storm. In the Asian sector, they compared mid-latitude stations Wuhan (Northern Hemisphere) and Yar2 (Southern Hemisphere) with the low-latitude station Cusv (Northern Hemisphere). They observed significant TEC decreases at mid-latitudes for several days post-storm but found TEC increased at low latitudes on the storm day with no subsequent decline. These results highlight the concentration of ionization at low latitudes near the equator following storms, while mid-latitudes experience significant reductions.

These results highlight the concentration of ionization at low latitudes near the equator following storms, while mid-latitudes experience significant reductions. According to results, based on these findings, our research aims to provide detailed insights into TEC disturbances at low latitudes, particularly in Bangkok and Chumphon, by leveraging GPS, IGS, and IRI data during the severe geomagnetic storms of March and April 2023 with the contribution of the understanding ionospheric behavior in equatorial regions and improving TEC disturbance modeling.

II. METHODOLOGY

Our research focused on TEC disturbances during two severe geomagnetic storms analyzed on March 24, 2023, and April 24, 2023, reported by the Space Weather Prediction Center (SWPC) as the second and third G4-class storms of Solar Cycle 25. These events marked the strongest geomagnetic storms in nearly six years. TEC data were analyzed from low-latitude GNSS receiver stations: THBK (13.729°N, 100.780°E) at King Mongkut's Institute of Technology Ladkrabang (KMITL) in Bangkok and THCP (10.724°N, 99.375°E) in Chumphon, Thailand. Data collection took place from March 21 to 29, 2023, and from April 20 to 28, 2023. The research methodology included the following steps:

1. Geomagnetic Storm Classification: Geomagnetic storm events were classified using the Planetarische Kennziffer (Planetary Index: Kp), Disturbance Storm Time (Dst) index, and Geomagnetic Auroral Electrojet (AE) index.

2. GNSS TEC Data Collection: GPS TEC data were extracted from Receiver Independent Exchange Format (RINEX) files obtained from GNSS receivers at THBK and THCP stations. Slant TEC (STEC) and Vertical TEC (VTEC) were calculated.

3. Supplementary TEC Data: IGS TEC data were acquired from IGS, and IRI TEC data were obtained from the International Reference Ionosphere (IRI).

4. Data Processing: The GPS TEC, IGS TEC, and IRI TEC were calculated using three-hour median values aligned with geomagnetic storm indices.

5. Data Analysis: The collected data were analyzed to evaluate TEC disturbances, and the findings were summarized.

This comprehensive approach provides insights into TEC behavior during severe geomagnetic storms at low latitudes, contributing to a better understanding of ionospheric dynamics.

A. GPS TEC Analysis

GPS TEC is derived by analyzing the delay in travel time of multi-frequency GPS signals received at GNSS stations. This involves both pseudorange and carrier phase measurements, which estimate the distance between GPS satellites and the receiver. The accuracy of these measurements depends not only on the satellite and receiver systems but also on environmental factors such as the ionosphere, troposphere, and multipath effects. The carrier phase measurements at L1 and L2 frequencies are calculated as follows.

$$L_1 = p - I_{p_1} + c(\tau^r_{p_1} - \tau^s_{p_1}) + T + \lambda_1 n_1 + \varepsilon_{L_1},$$
$$L_2 = p - I_{p_2} + c(\tau^r_{p_2} - \tau^s_{p_2}) + T + \lambda_2 n_2 + \varepsilon_{L_2}, \quad (1)$$

where L_1 and L_2 are carrier phase measured on the frequency of L_1 and L_2 respectively, p is geometrical range from satellite s to receiver r, τ^r is receiver clock error, τ^s is satellite clock error, T is a tropospheric delay, $I_{P1/2}$ are ionospheric delays in code measurement on $L_{1/2}$, $\lambda_{1/2} n_{1/2}$ are integer cycle ambiguities $\varepsilon_{P1/2}$ are multipath delays and other delays/errors in code measurement on $L_{1/2}$.

The L_1 and L_2 values for each GPS satellite are obtained from RINEX. Then, the STEC can be calculated in the next section. To map TEC measurements geographically, the thin shell model is used, representing the ionosphere as a spherical shell at a specific height (h). An elevation mapping function converts STEC measurements to VTEC values, which are then assigned to geographic locations based on the Ionospheric Pierce Point (IPP). The model assumes a shell height corresponding to the F2 peak density (hmF2) at approximately 400 km over Thailand (Kenpankho et al., 2011, p. 366). In GNSS systems like GPS, satellites transmit signals at multiple frequencies, such as f1 (1575.42 MHz) and f2 (1227.60 MHz). A GNSS receiver simultaneously receives signals from 4–12 satellites, allowing the computation of STEC values. $STEC_L$ is determined by calculating the differences between carrier phases (L1 and L2) of the two frequencies. These calculations are defined by Equations (2) (Blewitt, 1990, pp. 199–202; Kenpankho et al., 2011, p. 366).

$$\mathrm{STEC_L} = \frac{2\left(f_1 f_2\right)^2}{k\left(f_1^2 - f_2^2\right)}\left(L_1\lambda_1 - L_2\lambda_2\right), \quad (2)$$

where k, related to the ionosphere refraction, is 80.62 (m^3/s^2), λ_1, and λ_2 (λ_1 = 0.1904 m, λ_2 = 0.2444 m) are the wavelengths corresponding to f_1 and f_2, respectively.

VTEC represents the total number of electrons (in electrons per square meter; el/m²) in a vertical column with a one-square-meter cross-section (Goodwin et al., 1995, pp. 1723–1732). For GPS TEC, this refers to VTEC measured at the Ionospheric Pierce Point (IPP), accounting for the obliquity factor (Brunini et al., 2004, pp. 415–429). VTEC, in el/m², is derived from GPS STEC measurements by applying the obliquity factor, as shown in Equation (3) (Kenpankho et al., 2011, p. 366; Ma & Maruyama, 2003, p. 2084).

$$\mathrm{VTEC} = \mathrm{STEC}_L \times \cos\chi, \quad (3)$$

The zenith angle (χ) is the angle between a given location on the Earth's surface and the vertical direction pointing directly overhead. It is measured from the zenith, which is the point in the sky directly above an observer. The zenith angle (χ) is expressed from Equation (4) as

$$\chi = \arcsin\left(\frac{R_E \cos\alpha}{R_E + h}\right), \quad (4)$$

where R_E is the mean radius of the Earth, approximately 6,371 km, α is the elevation angle of the satellite, and h is the height of the ionospheric layer, which is assumed to be 400 km (Kenpankho et al., 2011, p. 366; Ma & Maruyama, 2003, p. 2084)

B. IGS TEC data

The IGS TEC, which stands for ionospheric TEC, is managed and supervised by the IGS organization. The IGS utilizes a global network of more than 515 GNSS data stations that operate continuously and provide high-quality multi-frequency data. The IGS has been recognized as an official service of the International Association of Geodesy (IAG) since 1994. It has also been a member of the Federation of Astronomical and Geophysical Data Analysis Services (FAGS) since 1996. The IGS is responsible for collecting, archiving, and distributing GPS observation data sets. Additionally, the IGS offers TEC map data, which is accessible through the File Transfer Protocol (FTP) for users to access and utilize. The IGS TEC data can be accessed through their FTP site at: https://igs.org. We selected the available IGS station located at CUUT00THA, Bangkok, Thailand (13.736°N, 100.534°E). There is also a station close to THBK, station (13.729°N, 100.780°E). The CPNM00THA, Chumphon, Thailand (10.725°N, 99.374°E) was chosen because it is located close to the THCP station (10.724°N, 99.375°E). We collected IGS TEC data for a total of nine days, starting three days before the severe geomagnetic storm occurred and continuing for five days after the severe geomagnetic storm occurred. Lastly, we analyzed the IGS TEC data during geomagnetic storm events based on the Dst, AE, and Kp indices time using the median statistic. The results of the IGS TEC data analyzed are presented in the following section.

C. IRI TEC data

The IRI is an organization established to develop an international standard for ionospheric parameters identifying. This standard is based on comprehensive data obtained from ground-based and satellite observations and it was initiated by the Committee on Space Research (COSPAR) and the International Union of Radio Science (URSI) in the late 1960s (Bilitza & Rinisch, 2008, pp. 599-609). TEC can be obtained from the IRI model, and it is referred to as IRI TEC. The IRI model is continually upgraded as new data and new modeling methods become available. This process has resulted in several milestone editions of the IRI (Bilitza, 1990, pp. 1–146; Bilitza, 2001, pp. 261-275; Bilitza & Rawer, 1996, pp. 735-772; Bilitza & Reinisch, 2008, pp. 599-609; Rawer et al., 1978a, pp. 177-181; Rawer et al., 1978b, pp. 6.1-6.10). Currently, the IRI-2020 is a new and improved empirical standard model of the ionosphere, addressing the limitations of its predecessors. The IRI-2020, the new empirical standard model of the ionosphere, is accessible at the following website: https://kauai.ccmc.gsfc.nasa.gov/instantrun/iri/. IRI TEC data were collected three days before the severe geomagnetic storm happened and five days after the severe geomagnetic storm happened, nine days in total. We input the location, date, and time to match the specific station's location and the period of the geomagnetic storm occurrence. In the final step, we analyzed the IRI TEC data, specifically focusing on the geomagnetic storm events that occurred during the designated periods according to the Dst, AE, and Kp indices. The analysis was performed using the median statistic. The results of the IRI TEC data analysis are presented in the next part.

D. Geomagnetic storm data

On March 24, 2023, the SWPC reported observing the second severe geomagnetic storm (G4) in solar cycle 25, which was the largest such event in nearly six years. The aurora was visible in more than half of the United States, reaching as far south as New Mexico, Missouri, and North Carolina. The second severe geomagnetic storm in 2023 occurred on Sunday, April 23, 2023, and continued until April 24, 2023, causing rare auroras to sparkle across Germany and France. Therefore, the geomagnetic storm data were collected for the periods of March 21-29, 2023, and April 20-28, 2023. We collected data for a total of nine days: three days before the severe geomagnetic storms occurred and five days after the severe geomagnetic storms occurred according to the TEC disturbances. The hourly equatorial Dst values can be found at https://wdc.kugi.kyoto-u.ac.jp/dst_realtime/index.html for geomagnetic storm indicators. AE index data were collected from the WDC for Geomagnetism Kyoto at https://wdc.kugi.kyoto-u.ac.jp/ae_realtime/index.html. The Kp index is a measure of geomagnetic activity on Earth, ranging from 0 to 9, with higher values indicating more significant geomagnetic disturbances and potential for brighter auroras. The Kp index geomagnetic storms were collected from the National Oceanic and Atmospheric Administration (NOAA), SWPC at the website https://www.swpc.noaa.gov/. The Kp index, which ranges from 0 to 9 in one-third increments, represents the average of the Ks indices obtained from 13 contributing geomagnetic observatories located at sub-auroral latitudes, collectively known as Kp stations.

E. Correlation coefficient

We also analyzed the correlation coefficient between geomagnetic storm levels and TEC values, including GPS TEC, IGS TEC, and IRI TEC. Correlation coefficient (r), which quantifies the linear relationship between variables x (geomagnetic storm level) and y (TEC values), and is calculated using Equation (5) (Mukaka, 2012, p. 69).

$$r = \frac{\sum_{i=1}^{n}(x_i - x)(y_i - y)}{\sqrt{\left[\sum_{i=1}^{n}(x_i - \bar{x})^2\right]\left[\sum_{i=1}^{n}(y_i - \bar{y})^2\right]}} \quad (5)$$

In this context, *r* signifies the correlation coefficient of the linear association between the variables *x* and *y*., x_i represents the geomagnetic storm scale value in a sample, $\bar{x}$ signifies the mean of the geomagnetic storm scale values, y_i indicates the TEC values in a sample, and $\bar{y}$ denotes the mean of the TEC values.

III. RESULTS

A. Geomagnetic storm levels

The results of the geomagnetic storm data analysis are plotted in Figures 1 and 2.

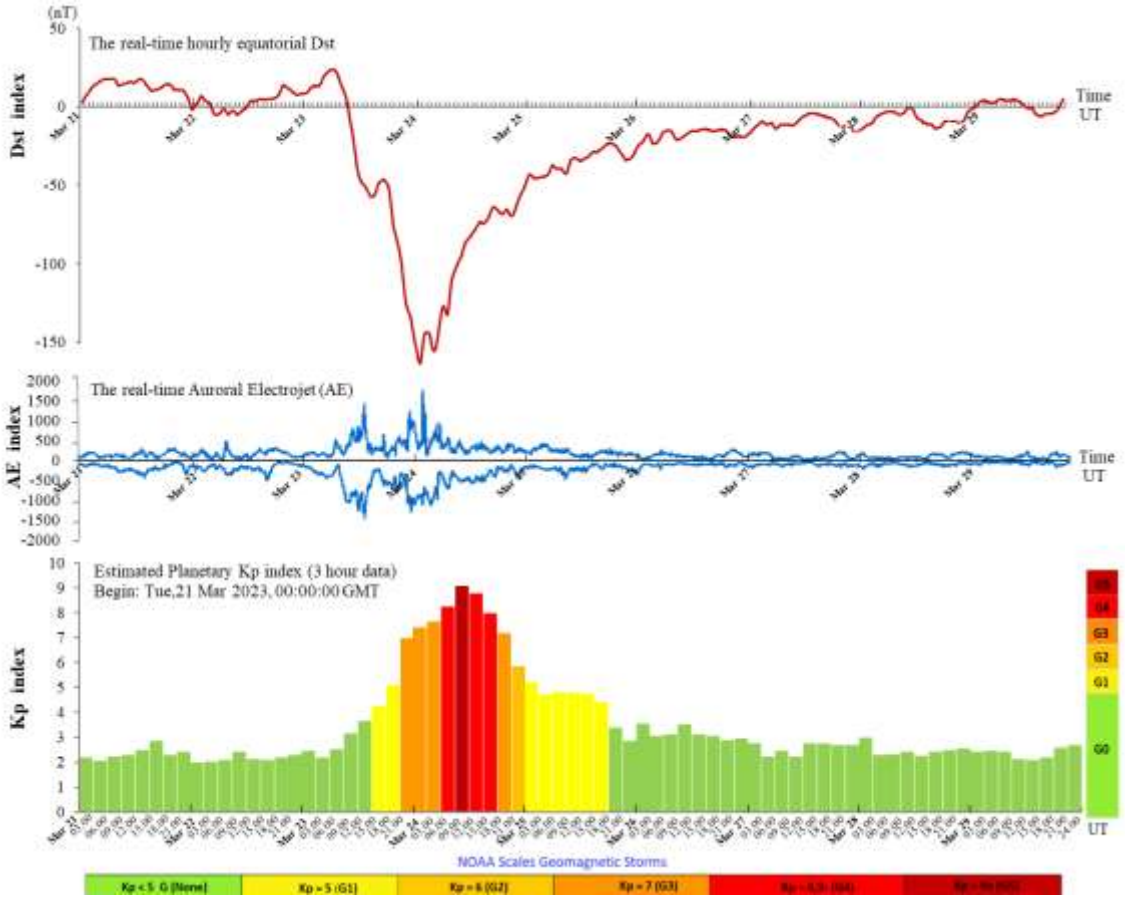

Figure 1: The Dst, AE, and Kp indices of the G4 severe geomagnetic storm that occurred from March 21-29, 2023.

Figure 1, the geomagnetic storm intensified from G1 (Kp = 5), G2 (Kp = 6), and G3 (Kp = 7) levels continuing into the late hours of March 23rd. On March 24th, the average intensity of the geomagnetic storm reached G4 level (Kp = 8,9-). Subsequently, the storm intensity decreased on March 25th and returned to normal on the following day. On March 23, 2023, solar activity was recorded at very low levels over the past 24 hours. According to SWPC's report, there were five numbered sunspots. The forecast indicated that solar activity would remain low with a slight chance of a flare on days one, two, and three following the geomagnetic storm days (24th, 25th, and 26th March). On March 28, 2023, the sun emitted a strong solar flare, which reached its peak as observed by the National Aeronautics and Space Administration (NASA)'s Solar Dynamics Observatory.

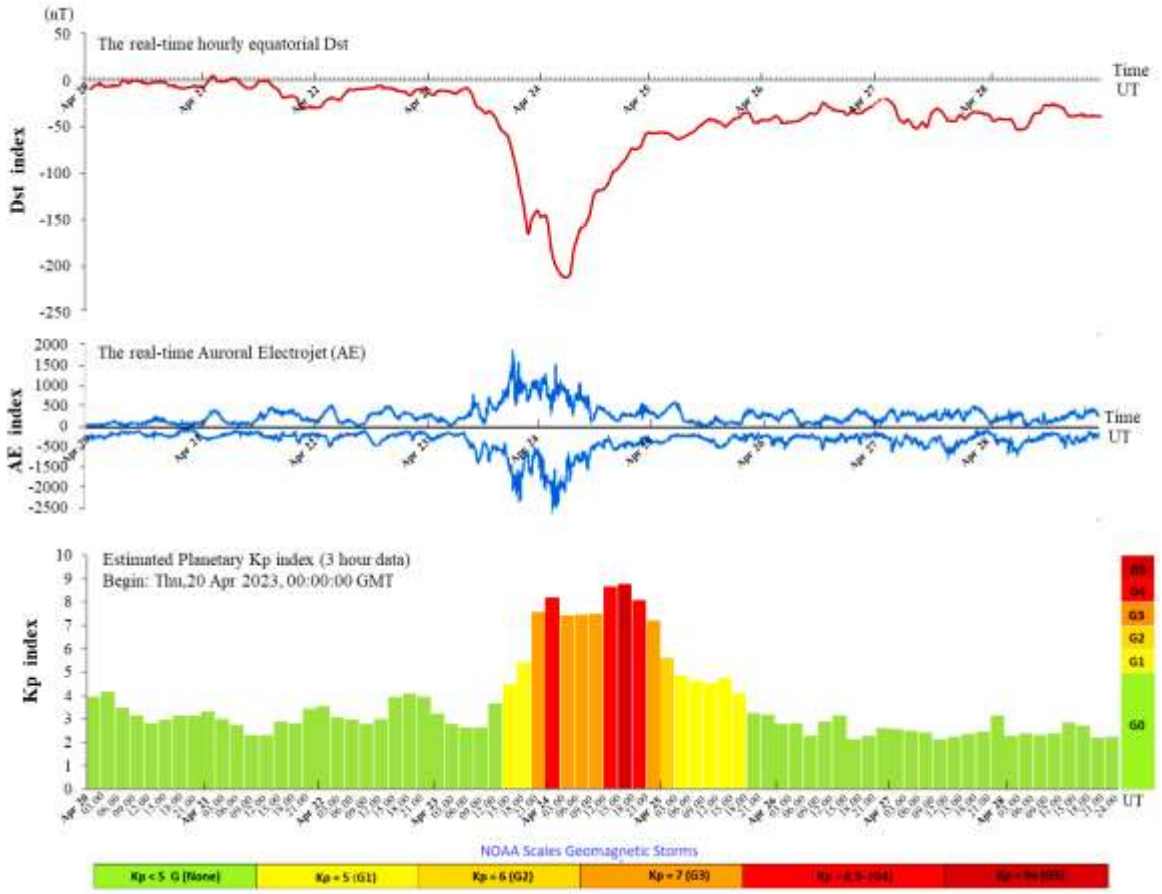

Figure 2: The Dst, AE, and Kp indices of the G4 severe geomagnetic storm that occurred from April 20-28, 2023.

Figure 2 illustrates the geomagnetic storm data collected from April 20-28, 2023. The graph revealed that the geomagnetic storm watches were in effect from April 23 to April 24, 2023. During this storm period, the storm intensified, reaching G1 (Kp = 5), G2 (Kp = 6), and G3 (Kp = 7) levels, and this continued into the late hours of April 23. On the night of April 23, the G3 period occurred and intensified further on April 24, reaching extreme storm at the G5 (Kp = 90) level. The average intensity of geomagnetic storms on April 24 was classified as a severe storm at the G4 (Kp = 8,9-). After that, the storm intensity gradually decreased on April 25 and returned to normal levels on the next day.

B. TEC disturbances during the storm time

After analyzing the data from GPS TEC, IGS TEC, and IRI TEC, we plotted the TEC data against the Dst, AE, and Kp indices as shown in Figures 3 and 4. There are GPS TEC, IGS TEC, and IRI TEC, which were observed during March 21-29, 2023, at the THBK station and during April 20-28, 2023, at the THCP station. The results indicated the notable significance of TEC anomalies during the geomagnetic storm day compared to the quiet geomagnetic stormy days, as shown in Figures 3 and 4.

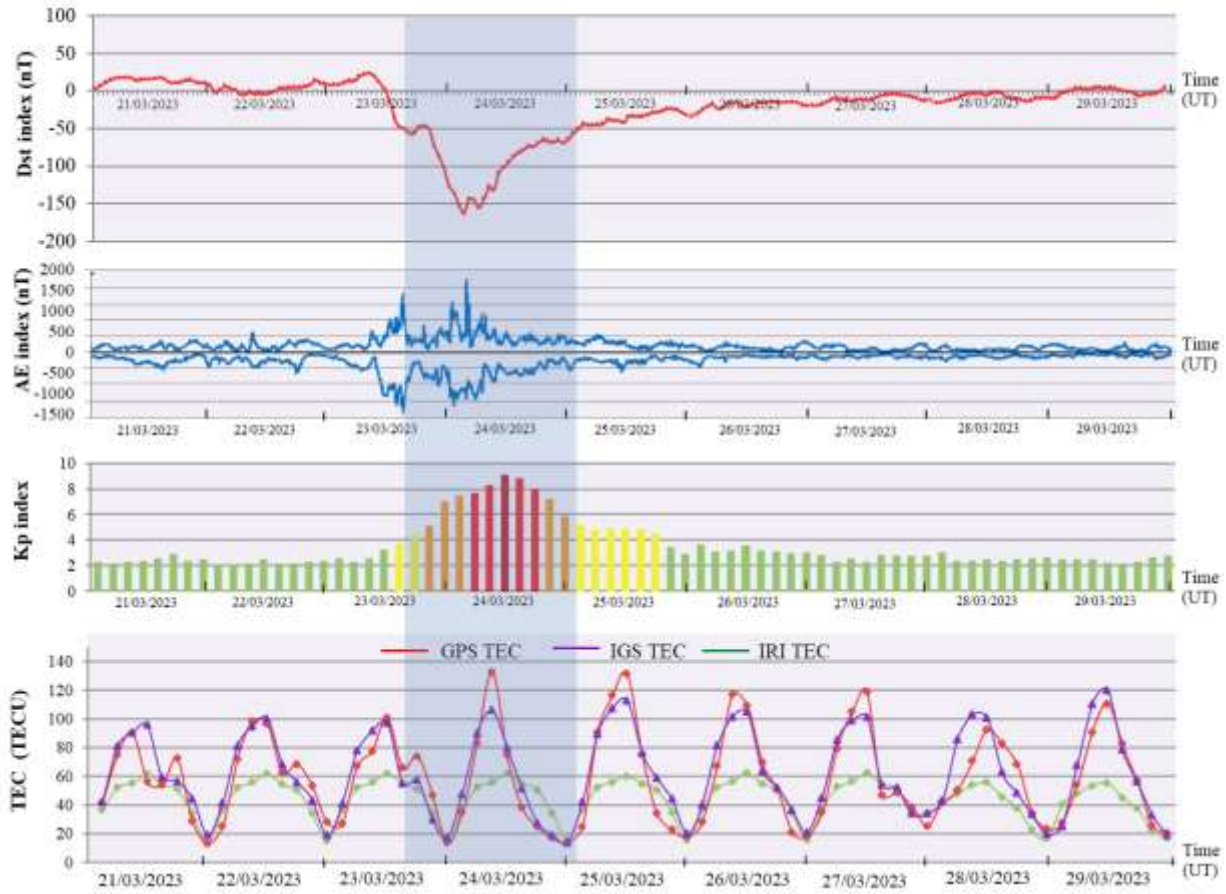

Figure 3: Anomalous TEC was observed over Bangkok, Thailand, during the period of severe geomagnetic storm from March 21-29, 2023.

Figure 3 presents a time series analysis of geomagnetic activity and TEC variations over the period from 21 to 29 March 2023. The four panels illustrate the Dst index, AE index, Kp index, and TEC values derived from GPS, IGS, and IRI models, respectively. In the first panel, the Dst index shows a pronounced drop reaching at –163 nT on 24 March 2023, indicating a strong geomagnetic storm. This sharp decrease highlights the main phase of the storm, which is also marked by the shaded region in the figure. The second panel displays the AE index, reflecting auroral electrojet activity. A significant spike occurs concurrently with the Dst minimum, confirming intense auroral activity during the storm period. In the third panel, the Kp index rises dramatically, peaking at Kp 8, which also indicates severe geomagnetic storm conditions. The elevated Kp levels persist for several hours on 24 March, aligning with the storm's peak intensity. The fourth panel illustrates TEC variations at a low-latitude station using three data sources: GPS TEC (red line), IGS TEC (purple line), and IRI TEC (green line). A substantial increase in TEC was observed on 24 March, particularly in the GPS and IGS data, with values peaking at above 120 TECU, compared to average daily peaks around 80-100 TECU during quieter days. This enhancement corresponds closely with the peak geomagnetic activity, suggesting a strong ionospheric response to the storm. The data presented that during geomagnetic storm-time activities, TEC tends to increase on the day of a severe storm that occurred on March 24, 2023. TEC remains high in the following days. Afterward, it gradually decreases back to normal levels within 2-3 days later. During the geomagnetic storm days, GPS TEC increased by approximately 10-35% compared to the 9-day average.

Figure 4: Anomalous TEC was observed over Chumphon, Thailand, during the period of severe geomagnetic storm from April 20-28, 2023.

Figure 4 compares geomagnetic storm activity and TEC variations from 20 to 28 April 2023. The data are presented in four panels: Dst index, AE index, Kp index, and TEC values from three sources: GPS, IGS, and IRI models. The shaded region highlights the period of the geomagnetic storm. In the first panel, the Dst index reaches a minimum value of –213 nT on 24 April 2023, indicating the main phase of an intense geomagnetic storm. This drop marks a strong disturbance in Earth's magnetic field. The second panel displays the AE index, representing auroral electrojet activity. A noticeable spike occurs concurrently with the Dst minimum, suggesting elevated auroral activity during the storm period. The third panel shows the Kp index, which reflects global geomagnetic activity. The Kp values peak at level 8 (G4) on 24 April, which signifies a severe geomagnetic event. Elevated Kp levels are observed from 23 to 25 April, confirming the duration and intensity of the storm. In the fourth panel, the TEC values are plotted from three sources: GPS TEC (red line), IGS TEC (purple line), and IRI TEC (green line). A significant TEC enhancement is evident on 24 April, with GPS TEC values peaking at approximately 175 TECU, much higher than the average on surrounding days. This increase corresponds with the timing of the geomagnetic storm, indicating a strong ionospheric response, particularly at low latitudes. The severe geomagnetic storm on April 24, 2023, is shown. TEC increases significantly on the day of the storm and begins to decrease the following day, gradually returning to normal

levels over the next few days. During the periods of geomagnetic storms, the GPS TEC increased by approximately 75% relative to the 9-day average.

Figures 5 and 6 present the Global Ionosphere Maps (GIMs) TEC during the severe geomagnetic storms of March 21–26, 2023, and April 20–25, 2023.

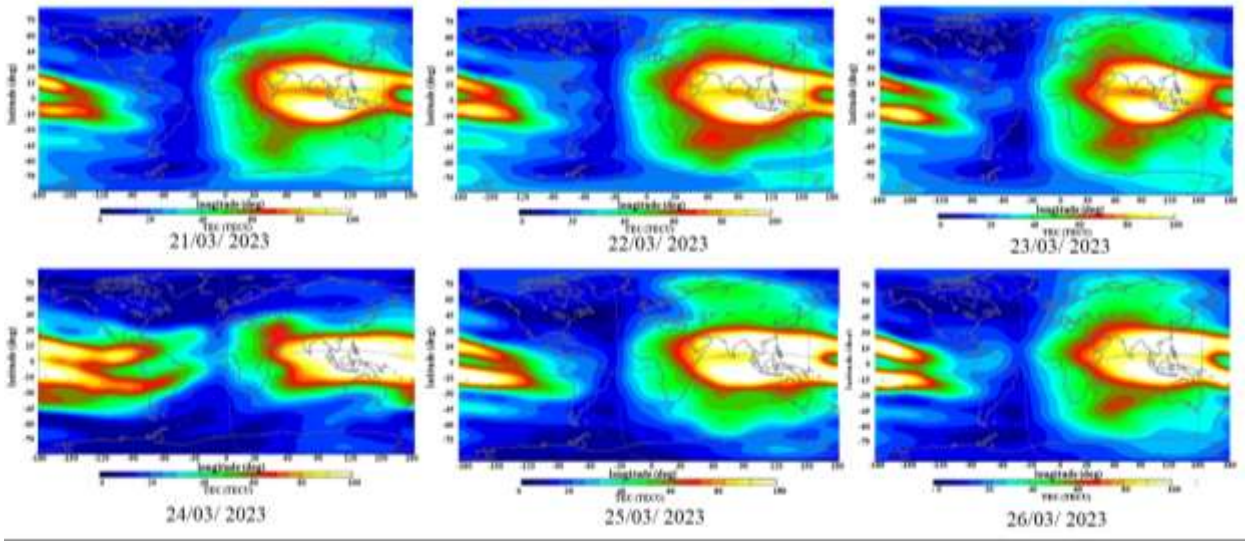

Figure 5 : The GIMs TEC during the severe geomagnetic storm period from March 21-26, 2023.

Figure 5 displays global TEC maps for six consecutive days, from 21 to 26 March 2023. Each map illustrates the spatial distribution of TEC values, measured in TEC units (TECU), with a color scale ranging from dark blue (low TEC) to red and white (high TEC). The maps focus particularly on the equatorial region, with the Southeast Asian sector, including Thailand, highlighted for reference. On 21 and 22 March, the TEC distribution appears relatively uniform with moderate intensity near the equatorial anomaly zones. There is a clear formation of EIA crests around ±15° magnetic latitude, especially over Southeast Asia. On 23 March, corresponding with a G2-class geomagnetic storm, there is a notable decrease in TEC intensity over the region, particularly around Thailand. The red and orange zones, indicating higher TEC values, are less pronounced, suggesting ionospheric disturbance. In contrast, the TEC maps for 24 and 25 March, which coincide with G4 and G2-class storms, respectively, exhibit a significant enhancement in TEC values. The equatorial anomaly intensifies, with brighter red and white zones expanding westward and eastward, indicating strong ionospheric activity likely driven by geomagnetic storm effects. By 26 March, the TEC pattern returns to a more moderate state, with the equatorial anomaly becoming more symmetric and the intensity decreasing compared to the peak seen on 24–25 March. Overall, the maps illustrate the dynamic response of the ionosphere to geomagnetic activity, particularly showing how storm intensity influences TEC variations across different longitudes and latitudes. These visualizations support the correlation analysis shown in the previous table, highlighting the significant TEC disturbances that occurred during strong geomagnetic storm events.

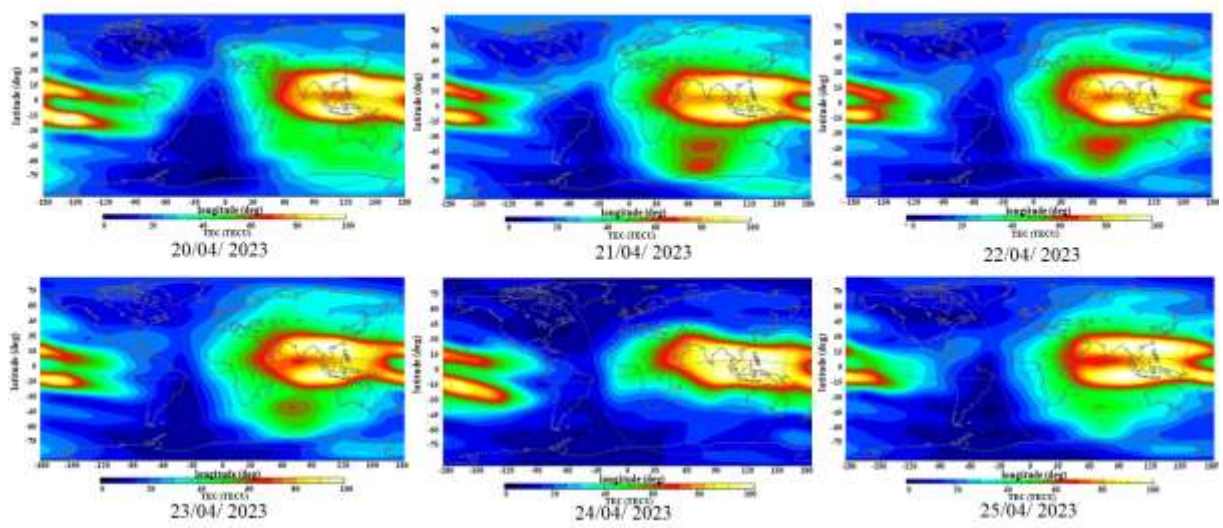

Figure 6: The GIMs TEC during the severe geomagnetic storm period from April 20-25, 2023.

Figure 6 illustrates global Total Electron Content (TEC) distributions over six consecutive days, from 20 to 25 April 2023. The TEC values, expressed in TEC units (TECU), are represented using a color scale from dark blue (low TEC) to red and white (high TEC). These maps highlight ionospheric conditions, particularly around the equatorial and low-latitude regions, with Thailand prominently marked as a reference location. On 20 April, the TEC distribution appears relatively moderate with a slight improvement around the equatorial region. Moving to 21 and 22 April, the maps show an increase in TEC intensity, particularly over Southeast Asia and the Pacific sector, indicating enhanced ionospheric activity likely associated with variations in space weather. The TEC map for 23 April, which corresponds with a G1-class geomagnetic storm, displays a further increase in TEC values, with intensified red zones and stronger Equatorial Ionization Anomaly (EIA) structures observed on both sides of the magnetic equator. The enhancement appears more asymmetric, suggesting storm-time ionospheric disturbances. On 24 April, during a G4-class geomagnetic storm, there is a pronounced increase in TEC levels, especially in the Southeast Asia–Pacific sector. The EIA becomes more intense and widespread, indicating a significant ionospheric response to strong geomagnetic activity. By 25 April, the TEC pattern shows signs of moderation, though high TEC values are still evident, particularly in regions west of the Pacific. This suggests a gradual return to quieter ionospheric conditions following the intense storm event. In summary, these maps demonstrate the temporal and spatial evolution of TEC during periods of geomagnetic activity. The strongest TEC disturbances are observed on 23 and 24 April, coinciding with the G1 and G4 storm levels, respectively. These findings align with the statistical correlation results and reinforce the impact of geomagnetic storms on ionospheric variability in low-latitude regions such as Thailand.

C. The correlation between geomagnetic storm levels and TEC disturbances

Table 1: Correlation coefficient between geomagnetic storm levels and TEC disturbances.

Correlation Coefficient (r) between TEC Disturbances and Geomagnetic Storm Levels							
THBK station, Bangkok				THCP station, Chumphon			
Storm Levels	GPS TEC	IGS TEC	IRI TEC	Storm Levels	GPS TEC	IGS TEC	IRI TEC
21/03/23 (G0)	-0.072	-0.398	-0.068	20/04/23 (G0)	-0.398	-0.304	0.344
22/03/23 (G0)	-0.035	-0.061	-0.182	21/04/23 (G0)	-0.792	-0.773	-0.518
(23/03/23) (G2)	-0.825	-0.900	-0.901	22/04/23 (G0)	-0.711	-0.819	-0.894
24/03/23 (G4)	0.482	0.595	0.955	23/04/23 (G1)	0.544	0.620	0.944
25/03/23 (G2)	0.818	0.905	0.978	24/04/23 (G4)	-0.116	-0.496	-0.118
26/03/23 (G0)	0.769	0.762	0.687	25/04/23 (G2)	0.321	0.327	0.792
(27/03/23) G0	-0.832	-0.847	-0.574	(26/04/23) G0	0.232	0.228	0.398
28/03/23 (G0)	-0.498	-0.501	-0.324	27/04/23 (G0)	-0.722	-0.744	-0.663
29/03/23 (G0)	-0.763	-0.639	-0.686	28/04/23 (G0)	-0.523	-0.488	-0.130

Table 1 presents the correlation coefficients (r) between geomagnetic storm levels and TEC disturbances, as observed at two GNSS stations in Thailand: THBK station in Bangkok and THCP station in Chumphon. The TEC data are categorized into three sources GPS TEC, IGS TEC, and IRI TEC across multiple dates in March and April 2023. For the THBK station in Bangkok, the table shows both positive and negative correlations, varying according to storm intensity and date. Notably strong negative correlations occurred on March 23, 2023 (G2 storm), with coefficients of -0.825 (GPS TEC), -0.900 (IGS TEC), and -0.901 (IRI TEC), indicating a significant inverse relationship between geomagnetic storm intensity and TEC values on that day. In contrast, strong positive correlations were observed during March 24, 2023 (G4) and March 25, 2023 (G2), with the IRI TEC correlation peaking at 0.978 on 25 March. These results suggest that the impact of geomagnetic storms on TEC disturbances can vary significantly, even from one day to the next. Similarly, at the THCP station in Chumphon, high positive correlations are evident on April 23, 2023 (G1 storm), with coefficients of 0.544 (GPS TEC), 0.620 (IGS TEC), and 0.944 (IRI TEC), while strong negative correlations were found on April 22, 2023 (G0), particularly in the IRI TEC data (-0.894). The presence of both strong positive and negative values indicates complex interactions between geomagnetic activity and TEC behavior, which may differ between geographical locations and data sources. In general, the table highlights how the intensity of geomagnetic storms (ranging from G0 to G4) can influence TEC disturbances differently depending on the measurement method and location. This emphasizes the importance of analyzing multiple TEC data sources and stations to better understand the response of the ionosphere to space weather events.

IV. CONCLUSION AND DISCUSSION

In this study, the analysis of TEC behavior during severe geomagnetic storms (G4 level) in Solar Cycle 25 reveals a clear and measurable ionospheric response over low-latitude and near-equatorial regions. During storm occurrence periods, TEC values exhibit a noticeable increase followed by a gradual return to baseline levels within a few days. Specifically, TEC values increased by approximately 10–35% at the THBK station in Bangkok, located in the low-latitude region, and up to 75% at the THCP station in Chumphon, situated near the equatorial region. This demonstrates that geomagnetic storms significantly impact ionospheric TEC, particularly at lower latitudes where the equatorial ionization anomaly plays a crucial role. These findings align with previous studies. For instance, Chen et al. (2017, pp. 3632–3639) analyzed ionospheric TEC variations under both quiet and disturbed geomagnetic conditions using SWM and RMC methodologies. Their results showed an overestimation of disturbance occurrences by approximately 5–20% during storm periods, and up to 35% during quiet periods. In comparison, our study found TEC enhancements of more than 75% (THCP station) and 10-35% (THBK station) in near-equatorial regions highlighting the regional sensitivity to geomagnetic disturbances. Similarly, Jenan et al. (2021, pp. 575–587) investigated ionospheric TEC responses to the September 2017 geomagnetic storm and December 2019 annular solar eclipse over Sri Lanka. Their findings showed a TEC enhancement of approximately 11 TECU during the main phase of the storm, with the most significant variation observed at Kegalle. In contrast, our study found TEC values reaching up to 10-75 TECU on the storm day, further emphasizing the intense ionospheric impact in equatorial regions during G4-level storms.

With regard to the correlation analysis, the correlation coefficients (r) between geomagnetic storm levels and TEC disturbances demonstrate a significant and positive relationship. This indicates that the intensity of geomagnetic storms is strongly associated with TEC variability, particularly during G2-G4 level events. Higher storm levels tend to correspond with increased TEC values, reaffirming the sensitivity of the ionosphere to geomagnetic forcing in low-latitude and equatorial zones. Our results are also consistent with Nava et al. (2016, pp. 3421–3438), who studied ionospheric responses at mid- and low-latitudes. Their research reported an initial increase in TEC on storm days, followed by a subsequent decrease over several days, especially at mid-latitudes. However, at low latitudes, as similarly shown in our study, no post-storm reduction in TEC was observed, and enhancement patterns were more sustained.

In conclusion, the current study confirms that TEC variations are closely linked to geomagnetic storm intensity, with stronger storms yielding greater enhancements, especially in regions near the equator. This emphasizes the need for continuous monitoring of ionospheric behavior during space weather events to support GNSS-based applications in low-latitude countries like Thailand.

ACKNOWLEDGEMENT

We would like to thank the Institute of Geology and Geophysics, Chinese Academy of Sciences (IGGCAS), and the Earthquake Observation Division (EOD), Thai Meteorological Department (TMD) for supporting the BG2s GNSS receiver and sharing data. We would like to thank the International Reference Ionosphere (IRI) for IRI TEC and the International GNSS Service (IGS) for IGS TEC Maps for sharing data. We would like to thank the Space Weather Prediction Center (SWPC), and the National Oceanic and Atmosphere Administration (NOAA) organization for sharing data on geomagnetic storm activity. We would like to thank the World Data Center (WDC) for Geomagnetism, Kyoto, Japan, for sharing the AE and Dst indices data.

REFERENCES

Adolfs, M., Hoque, M. M., & Shprits, Y. Y. (2022). Storm-time relative total electron content modelling using machine learning techniques. *Remote Sensing, 14*(23), 1-17.

Ali, O. H., Zaourar, N., Fleury, R., & Amory-Mazaudier, C. (2021). Transient variations of vertical total electron content at low latitude during the period 2013–2017. *Advances in Space Research, 68*(12), 4857-4871.

Bilitza, D. (1990). *International Reference Ionosphere 1990 (Report no. NSSDC/WDC-A-R&S 90-22).* National Space Science Data Center *(*NSSDC) and World Data Center A for Rockets and Satellite (WDC-AR &S). https://ntrs.nasa.gov/api/citations/19910021307/downloads/19910021307.pdf.

Bilitza, D. (2001). International reference ionosphere 2000. *Radio Science, 36*(2), 261-275.

Bilitza, D., & Rawer, K. (1996). International Reference Ionosphere, in: W. Dieminger, G. Hartmann and R. Leitinger (Eds.), *The upper atmosphere - data analysis and interpretation* (pp. 735-772). Springer-Verlag.

Bilitza, D., & Reinisch, B. W. (2008). International Reference Ionosphere 2007: Improvements and new parameters. *Advances in Space Research, 42*(4), 599-609.

Blewitt, G. (1990). An automatic editing algorithm for GPS data. *Geophysical Research Letters, 17*(3), 199-202.

Bojilova, R., & Mukhtarov, P. (2023). Comparative analysis of global and regional ionospheric responses during two geomagnetic storms on 3 and 4 February 2022. *Remote Sensing, 15*(7), 1-23.

Brunini, C., Meza, A., Azpilicueta, F., Van Zele, M. A., Gende, M., & Díaz, A. (2004). A new ionosphere monitoring technology based on GPS. *Astrophysics and Space Science, 290*, 415-429.

Chen, Z., Wang, J. S., Deng, Y., & Huang, C. M. (2017). Extraction of the geomagnetic activity effect from TEC data: A comparison between the spectral whitening method and 28 day running median. *Journal of Geophysical Research: Space Physics, 122*(3), 3632-3639.

Chernyshov, A. A., Miloch, W. J., Jin, Y., & Zakharov, V. I. (2020). Relationship between TEC jumps and auroral substorm in the high-latitude ionosphere. *Scientific Reports, 10*(1), 1-13.

de Paula, E. R., de Oliveira, C. B., Caton, R. G., Negreti, P. M., Batista, I. S., Martinon, A. R., Neto, A. C., Abdu, M. A., Monico, J. F. G., Sousasantos, J., & Moraes, A. O. (2019). Ionospheric irregularity behavior during the September 6–10, 2017 magnetic storm over Brazilian equatorial–low latitudes. *Earth, Planets and Space, 71*(42), 1-15.

Dugassa, T., Habarulema, J. B., & Nigussie, M. (2019). Investigation of the relationship between the spatial gradient of Total Electron Content (TEC) between two nearby stations and the occurrence of ionospheric irregularities. In I. A. Daglis, C. Jacobi, & I. Mann (Eds.), *Annales Geophysicae* (Vol. 37, No. 6, pp. 1161-1180). Copernicus.

Goodwin, G. L., Silby, J. H., Lynn, K. J. W., Breed, A. M., & Essex, E. A. (1995). GPS satellite measurements: Ionospheric slab thickness and total electron content. *Journal of Atmospheric and Terrestrial Physics, 57*(14), 1723-1732.

Hofmann-Wellenhof, B., Lichtenegger, H., & Collins, J. (2012). Observables. In *Global positioning system: Theory and practice* (pp. 87-131). Springer-Verlag Wien GmbH.

Jenan, R., Dammalage, T. L., & Panda, S. K. (2021). Ionospheric total electron content response to September-2017 geomagnetic storm and December-2019 annular solar eclipse over Sri Lankan region. *Acta Astronautica, 180,* 575-587.

Kenpankho, P., Watthanasangmechai, K., Supnithi, P., Tsugawa, T., & Maruyama, T. (2011). Comparison of GPS TEC measurements with IRI TEC prediction at the equatorial latitude station, Chumphon, Thailand. *Earth, Planets and Space, 63*, 365-370.

Klimenko, M. V., Klimenko, V. V., Zakharenkova, I. E., Ratovsky, K. G., Korenkova, N. A., Yasyukevich, Y. V., Mylnikova, A. A., & Cherniak, I. V. (2017). Similarity and differences in morphology and mechanisms of the fo F2 and TEC disturbances during the geomagnetic storms on 26–30 September 2011. In *Annales Geophysicae* (Vol. 35, No. 4, pp. 923-938). Copernicus.

Kumar, K. V., Maurya, A. K., Kumar, S., & Singh, R. (2016). 22 July 2009 total solar eclipse induced gravity waves in ionosphere as inferred from GPS observations over EIA. *Advances in Space Research, 58*(9), 1755-1762.

Li, G., Ning, B., Zhao, X., Sun, W., Hu, L., Xie, H., Liu, K., & Ajith, K. K. (2019). Low latitude ionospheric TEC oscillations associated with periodic changes in IMF Bz polarity. *Geophysical Research Letters, 46*(16), 9379-9387.

Ma, G., & Maruyama, T. (2003, October). Derivation of TEC and estimation of instrumental biases from GEONET in Japan. In *Annales Geophysicae* (Vol. 21, No. 10, pp. 2083-2093). Copernicus.

Mansilla, G. A. (2019). Behavior of the Total electron content over the Arctic and Antarctic sectors during several intense geomagnetic storms. *Geodesy and Geodynamics, 10*(1), 26-36.

Mukaka, M. M. (2012). A guide to appropriate use of correlation coefficient in medical research. *Malawi Medical Journal, 24*(3), 69-71.

Nava, B., Rodríguez-Zuluaga, J., Alazo-Cuartas, K., Kashcheyev, A., Migoya-Orué, Y., Radicella, S. M., Radicella, C., Armory-Mazaudier, C., & Fleury, R. (2016). Middle-and low-latitude ionosphere response to 2015 St. Patrick's Day geomagnetic storm. *Journal of Geophysical Research: Space Physics, 121*(4), 3421-3438.

Nayak, C., Tsai, L. C., Su, S. Y., Galkin, I. A., Tan, A. T. K., Nofri, E., & Jamjareegulgarn, P. (2016). Peculiar features of the low-latitude and midlatitude ionospheric response to the St. Patrick's Day geomagnetic storm of 17 March 2015. *Journal of Geophysical Research: Space Physics, 121*(8), 7941-7960.

Pi, X., Mannucci, A. J., Lindqwister, U. J., & Ho, C. M. (1997). Monitoring of global ionospheric irregularities using the worldwide GPS network. *Geophysical Research Letters, 24*(18), 2283-2286.

Rao, S. S., Galav, P., Sharma, S., & Pandey, R. (2013). Low-latitude TEC variability studied from magnetically conjugate locations along 73° E longitude. *Journal of Atmospheric and Solar-Terrestrial Physics, 104*, 1-6.

Ratovsky, K. G., Klimenko, M. V., Dmitriev, A. V., & Medvedeva, I. V. (2022). Relation of extreme ionospheric events with geomagnetic and meteorological activity. *Atmosphere, 13*, 1-15.

Rawer, K., Bilitza, D., & Ramakrishnan, S. (1978a). Goals and status of the International Reference Ionosphere. *Reviews of Geophysics, 16*(2), 177-181.

Rawer, K., Bilitza, D., Ramakrishnan, S., & Sheikh, N. (1978b). Intentions and build-up of the International Reference Ionosphere. *Operational Modelling of the Aerospace Propagation Environment*, *1&2,* 6.1-6.10.

Reddy, C. A. (1986). The equatorial ionosphere. *Indian Journal of Radio & Space Physics, 15*(5&6), 247-263.

Reddybattula, K. D., Panda, S. K., Ansari, K., & Peddi, V. S. R. (2019). Analysis of ionospheric TEC from GPS, GIM and global ionosphere models during moderate, strong, and extreme geomagnetic storms over Indian region. *Acta Astronautica, 161*, 283-292.

Serafimov, K. B., Arshinkov, I. S., Bochev, A. Z., Petrunova, M. H., Stanev, G. A., & Chapkanov, S. K. (1982). A measuring equipment for electric and magnetic fields in the range of the ionosphere—Magnetosphere plasma mounted aboard the “Intercosmos-Bulgaria 1300” satellite. *Acta Astronautica, 9*(6-7), 397-399.

Skone, S., & de Jong, M. (2000). The impact of geomagnetic substorms on GPS receiver performance. *Earth, Planets and Space, 52*, 1067-1071.

Tsurutani, B. T., Lakhina, G. S., & Hajra, R. (2020). The physics of space weather/Solar-Terrestrial Physics (STP): what we know now and what the current and future challenges are. *Nonlinear Processes in Geophysics, 27*(1), 75-119.

Zhou, Y. L., Lühr, H., Xiong, C., & Pfaff, R. F. (2016). Ionospheric storm effects and equatorial plasma irregularities during the 17–18 March 2015 event. *Journal of Geophysical Research: Space Physics, 121*(9), 9146-9163.